NANO LETTERS

Letter

pubs.acs.org/NanoLett

Shrinking and Growing: Grain Boundary Density Reduction for Efficient Polysilicon Thin-Film Solar Cells

Dong Rip Kim,[†] Chi Hwan Lee,[‡] Jeffrey M. Weisse,[‡] In Sun Cho,[‡] and Xiaolin Zheng*[,‡]

[†]Department of Mechanical Engineering, Hanyang University, Seoul, 133-791, Korea

[‡]Department of Mechanical Engineering, Stanford University, California 94305, United States

Supporting Information

ABSTRACT: Polycrystalline Si (poly-Si) thin-film, due to its low Si consumption, low substrate cost, and good stability, is an attractive candidate for cost-effective solar cells, but the as-deposited poly-Si typically has a columnar structure with grain boundaries in between, severely limiting the efficiency of the poly-Si. Here, we report a micropillar poly-Si solar cell that utilizes the columnar structure of the as-deposited poly-Si grains. We first formed submicrometer diameter poly-Si pillars, smaller than the initial grain sizes, and used these pillars as the seeds for the subsequent epitaxial growth of Si, which effectively reduces grain boundary density in the final poly-Si crystal. In addition, the vertically aligned micropillar arrays form radial p−n junctions that further mitigate the grain boundary recombination losses by improving the light absorption and charge-carrier collection efficiencies. Consequently, the maximum efficiency of micropillar poly-Si thin-film solar cells is 6.4%, that is, ∼1.5 times higher than that of the planar cells.

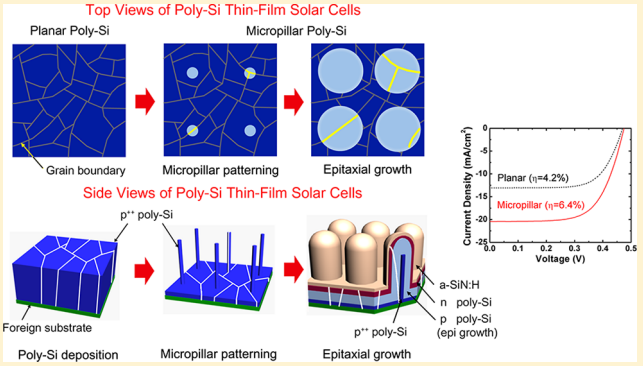

KEYWORDS: *Polycrystalline Si, micropillar-seeded growth, thin-film solar cells, radial junction, light trapping*

Poly-Si thin-film solar cells (TFSCs) fabricated on inexpensive substrates carry a promise both to lower the cost per watt compared to bulk Si wafer-based solar cells owing to significant reductions in Si consumption and substrate costs, and to have better light soaking stability than amorphous Si (α-Si).[1−8] Poly-Si TFSCs are typically deposited on foreign substrates by two deposition methods: direct deposition of poly-Si,[2−4] and first deposition of α-Si followed by recrystallization techniques to form poly-Si.[6−10] Both deposition methods have the advantages of high throughput and scalability,[1,7,8] but the formed poly-Si thin-film typically has a columnar grain structure that acts as charge-carrier recombination sites, leading to large leakage current.[4,9,10] Here, we take advantage of the columnar structure of the as-deposited poly-Si thin-film and report a poly-Si micropillar-seeded growth of TFSCs that have (1) enlarged effective grain sizes by reducing grain boundary density, (2) reduced charge-carrier collection distance, and (3) enhanced light absorption. All of the three features of our poly-Si TFSCs reduce the charge-carrier recombinations occurring at the boundaries between columnar grains. The efficiency of micropillar poly-Si TFSCs exhibits up to 6.4%, that is, about 1.5 times higher than that of the control planar poly-Si solar cells.

The design and fabrication of our micropillar poly-Si TFSCs are illustrated in Figure 1. First, a heavily doped p^{++} poly-Si thin-film (about 18 μm thick, grain size of 3.9 ± 0.5 μm) with columnar grain structures was deposited on a 600 nm thick thermal oxide layer on top of a 500 μm thick Si wafer (Figure 1a, left), which was used for the purpose of resembling foreign substrates and can be replaced by other cheaper substrates (e.g., alumina).[3] The p^{++} Si layer serves as a bottom surface passivation layer by forming the back surface field to the active p-type Si layer. Second, micrometer-size Si pillar arrays (3 μm diameter) were patterned by photolithography and formed by deep reactive ion etching. The Si micropillars were further shrunk by isotropic dry etching to smaller diameter pillars with diameters about 0.8−0.9 μm (Figure 1a, center, and Figure 1b, left), which is much smaller than the average grain size of 3.9 μm of the as-deposited Si (Figure 1b, left). As such, the resulting Si micropillars are either poly-crystalline Si with a few vertical grains or even single-crystalline Si, depending on where the micropillars were formed relative to the grain boundaries. Third, the p^{++} Si micropillars were used as the seeds for the subsequent epitaxial growth of a p-type Si thin-film for which the top layer was further doped to be n-type by dopant diffusion process to form a p−n junction (Figure 1a, right). Fourth, a 80 nm thick hydrogenated amorphous silicon nitride (a-SiN:H) was deposited as an antireflective and surface passivation layer by the plasma-enhanced chemical vapor deposition method (PECVD). Finally, Ti/Pd/Ag (5/300/700 nm) and Al (700 nm) layers were metalized as the top and bottom contact (mesa structure), respectively, by using an electron beam evaporator. The final vertical Si micropillar arrays have an average diameter of 6 μm, center-to-center

Received: November 9, 2012
Published: November 20, 2012

   dx.doi.org/10.1021/nl3041492 | *Nano Lett.* 2012, 12, 6485−6491

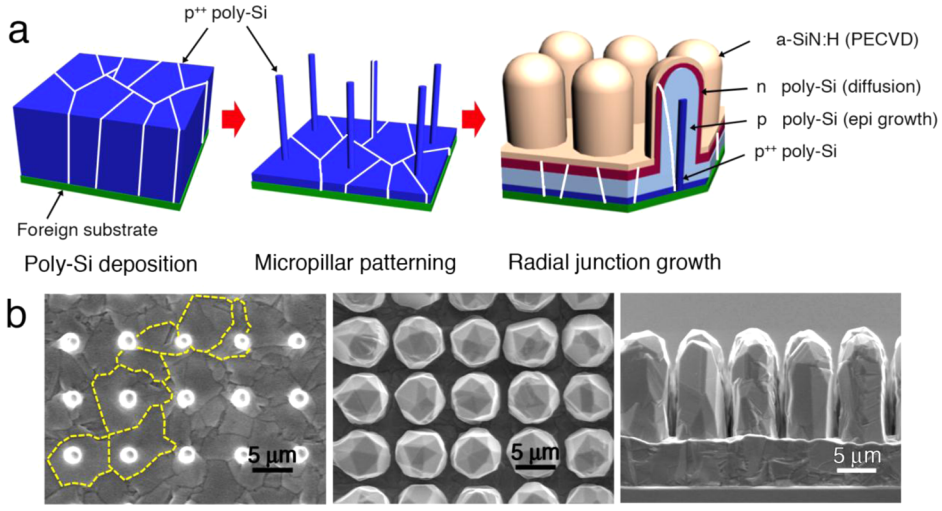

Figure 1. Micropillar poly-Si thin-film solar cells (TFSCs). (a) Schematics of the fabrication process of the micropillar poly-Si TFSCs. The p^{++} Si micropillars are formed by using dry etching of the p^{++} poly-Si thin-film deposited on foreign substrate. The patterned p^{++} micropillars are used as seeds for the subsequent growth of p-type poly-Si absorber, followed by the dopant diffusion process to form the radial p−n junction, and the deposition of the outermost a-SiN:H layer. (b) Scanning electron microscopy (SEM) images of the micropillar poly-Si TFSCs. (Left) The diameter of the p^{++} micropillars is smaller than the average grain size of the as-deposited poly-Si so that the micropillars are either single- or polycrystalline Si with a few vertical grains, depending on where the micropillars were formed relative to the grain boundaries (yellow dot). (Middle) Top view and (right) side view of the final micropillar poly-Si TFSCs.

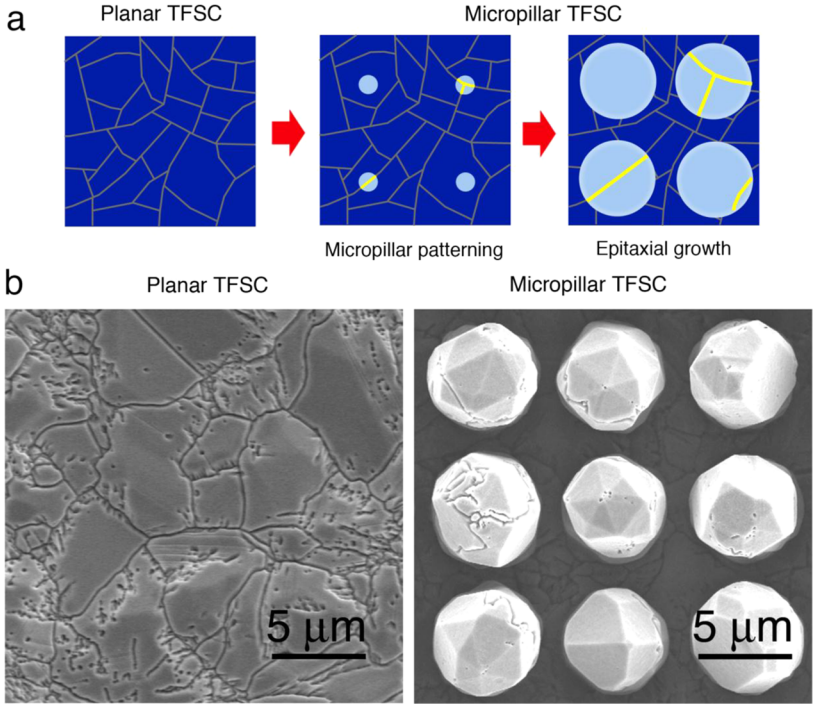

Figure 2. Enlarged grain size effects of the micropillar poly-Si TFSCs. (a) Schematics of the reduction of grain boundary density within the micropillars, compared to the planar thin-film: top views of planar p^{++} poly-Si thin-film (left), the p^{++} micropillar formation (middle), and the epitaxial growth of the p-type poly-Si (right). The p-type poly-Si grain growth mostly follows the grains of the p^{++} Si micropillars. (b) SEM images of the Secco-etched planar TFSCs (left) and the Secco-etched micropillar TFSCs (right).

spacing of 7 μm, and height of 15 μm (Figure 1b, middle and right) with a cell area of 1 cm^2. The detailed fabrication procedures and device configurations are described in the Methods section. Control planar poly-Si TFSCs were fabricated with identical processes except that the dry etching step for forming the Si micropillars was not carried out.

The micropillar solar cells have distinct advantages compared to the control planar cells in terms of material quality, charge-carrier collection, and light absorption efficiencies. First, since the p^{++} Si micropillars are shrunk to be much smaller than the initial grain size, they possess a few or even no grain boundaries (Figure 2a). The subsequent epitaxial deposition of p-type poly-Si absorber layer follows the grains of the p^{++} Si micropillars. Accordingly, the final micropillars have about half grain boundary density (i.e., grain boundary density = total grain boundary length/top projection area, $\sim 0.22 \pm 0.05\ \mu m^{-1}$)

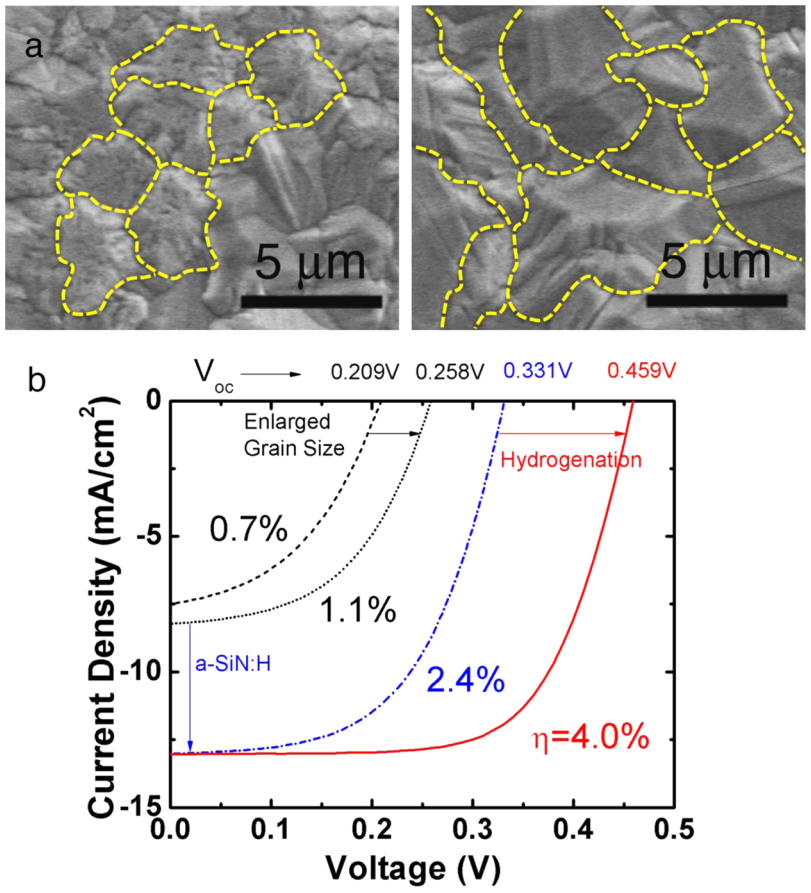

Figure 3. Optimization of the planar poly-Si TFSCs. (a) SEM images of the grain size enlargement from (left) to (right) of poly-Si thin-film by using the nucleation density control method (yellow dot: grain boundaries). (b) The photovoltaic properties of the planar poly-Si TFSCs are steadily improved by grain size enlargement (black dash and black dot), the inclusion of the top a-SiN:H layer (blue dash-dot), and the hydrogenation process (red solid).

than the planar one (~0.42 ± 0.02 μm^{-1}). The reduction in grain boundary densities within the micropillars is clearly seen in the SEM images in Figure 2b, where the grain boundaries were made more visible by using the Secco etching. The reduction of grain boundary density within the micropillars decreases the deleterious grain boundary recombination[11,12] and hence improves the photovoltaic properties of solar cells. Second, the radial junction structure of the micropillars has the recognized potential of achieving high solar power conversion efficiency by decoupling the direction of light absorption and charge-carrier collection to the long axial and short radial directions, respectively.[13,14] To date, such radial junction structures have been mainly applied to high-quality single-crystalline materials where it has limited benefits for improving charge-carrier collection.[14−16] Low-grade materials, such as poly-Si, can benefit more from the improved charge-carrier collection process due to their shorter minority carrier diffusion lengths. Finally, vertically aligned wire arrays have been extensively demonstrated to have enhanced light absorption due to the combined antireflection and increased scattering effects.[15,17] Our poly-Si micropillar arrays also have faceted tips (Figure 1b) that further enhance the antireflection effect due to the graded refractive index.[18]

To fully examine the merits of our micropillar poly-Si TFSCs over the control planar cells, we first optimized the fabrication process for the planar poly-Si TFSCs by using the established technologies, including enlarging the as-deposited poly-Si grain sizes, depositing an a-SiN:H antireflective layer, and carrying out hydrogenation. First, the as-deposited grain size can be increased by using the nucleation density control method, for which the hydrogen chloride (HCl) gas was introduced during the deposition of poly-Si to reduce the nucleation density of Si by etching the Si nuclei[3,4] so that the remaining nuclei had more room to grow larger before colliding with each other to form a grain boundary. It should be noted that the grain size of as-deposited poly-Si can also be increased by metal-induced crystallization.[2] Figure 3a shows that the average Si grain size is increased from 2.1 to 3.9 μm as the partial pressure of HCl gas is increased during the deposition of poly-Si. Accordingly, the efficiency (η) of the planar poly-Si thin-film solar cells increases from 0.7% to 1.1% (Figure 3b). Furthermore, the efficiency of the planar cells is more than doubled to 2.4% by the inclusion of the top a-SiN:H layer that provides combined antireflection, surface passivation, and defect passivation by atomic hydrogen during the PECVD process.[19] Finally, the efficiency of the planar cells is further improved to 4.0% by carrying out the hydrogenation process that effectively passivates defects with atomic hydrogen (see the Methods section)[20,21] and improves mainly the open circuit voltage (V_{oc}) and fill factor (FF) (Figure 3b). Our optimized fabrication process yields comparable photovoltaic performance to the state-of-the-art poly-Si TFSCs with similar configurations.[2] The photovoltaic performance of the planar poly-Si TFSCs can be further improved by using back surface reflector, heterojunction

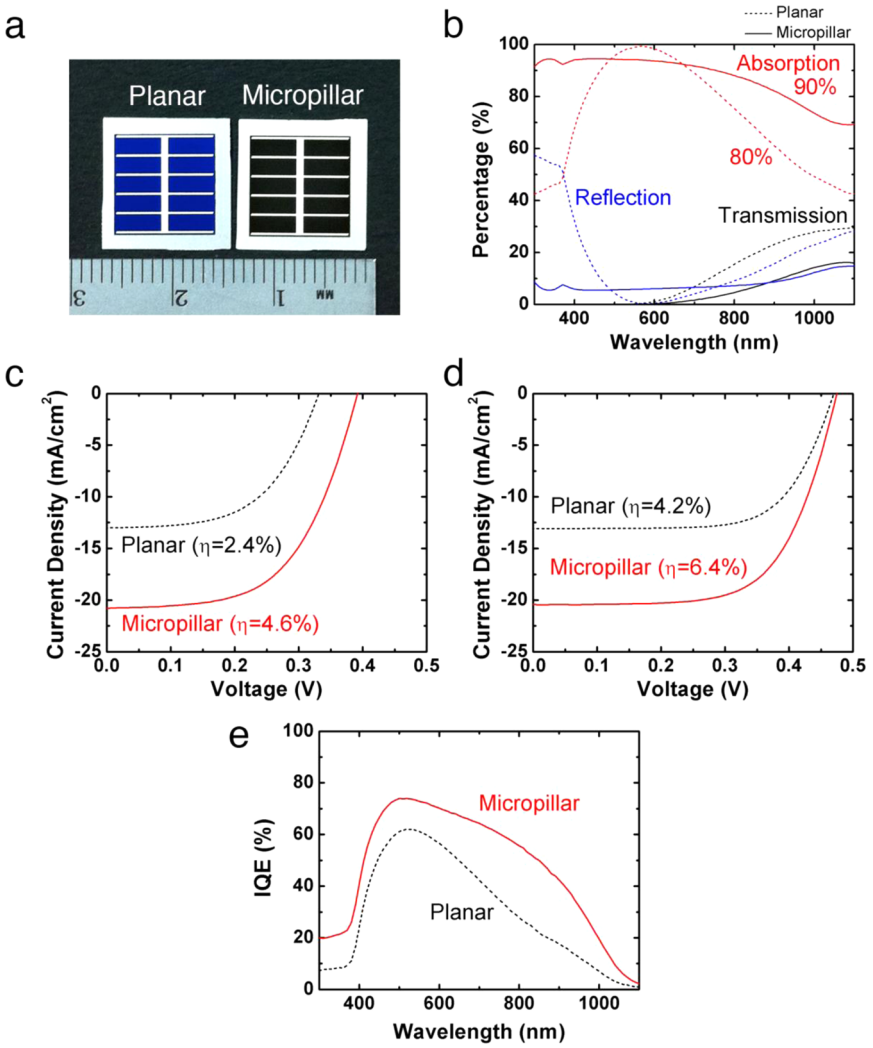

Figure 4. Comparisons of the micropillar to the planar poly-Si TFSCs. (a) Optical image of both TFSCs. (b) Light absorption (red), reflection (blue), and transmission (black) percentages of the micropillar (solid) and the planar (dash) poly-Si TFSCs as functions of wavelengths. (c) Light $J-V$ curves of the micropillar (red solid) and the planar poly-Si TFSCs (black dash) without the hydrogenation process. The micropillar solar cell exhibits the efficiency of 4.6% (V_{oc} of 0.392 V, J_{sc} of 20.8 mA/cm^2, and FF of 0.570), and the control planar cell has an efficiency of 2.4% (V_{oc} of 0.331 V, J_{sc} of 13.0 mA/cm^2, and FF of 0.557). (d) Light $J-V$ curves of the micropillar and the planar poly-Si TFSCs after the hydrogenation process. The micropillar solar cell (red solid) exhibits a maximum efficiency of 6.4% (V_{oc} of 0.475 V, J_{sc} of 20.4 mA/cm^2, and FF of 0.655), which is 1.5 times higher than that of the control planar solar cell (black dash, a maximum η of 4.2%: V_{oc} of 0.470 V, J_{sc} of 13.1 mA/cm^2, and FF of 0.677). (e) Internal quantum efficiency (IQE) as functions of the wavelength for the micropillar (red solid) and the planar solar cells (black dash) after the hydrogenation process.

structure, and interdigitated metal electrodes.[2] We did not carry out these additional optimization steps since we want to focus on the comparisons between planar and micropillar poly-Si TFSCs.

The photovoltaic properties of the micropillar poly-Si TFSCs are compared with those of control planar solar cells in Figure 4. The optical images (Figure 4a) show that the control planar solar cell is bluish while the micropillar solar cell colors black, indicating the micropillar solar cell has reduced light reflection. The light absorption measurement confirms that the micropillar absorbs about 90% light of air mass 1.5 global (AM 1.5G) spectrum above the band gap of Si due to the suppressed reflection and transmission, compared to about 80% for the planar cell (Figure 4b). It should be noted that the planar cell used for the light absorption measurement does not have the 18 μm thick p^{++} poly-Si layer so that we only accounted for the light absorption by the active layer, but the light absorption measurement of the micropillar included the 3 μm thick planar p^{++} poly-Si layer and 15 μm long p^{++} poly-Si micropillars that cannot be removed for the fabrication of micropillar solar cell. In other words, the total amount of light absorption of our micropillars by the active p-type poly-Si layers can be smaller than 90% that leaves room for further improvement by optimizing the geometry of the Si micropillar arrays.[17] The electrical characterization shows that the micropillar poly-Si TFSCs have apparent superior photovoltaic properties over the control planar cells (Figure 4c and d). The micropillar solar cell exhibits a maximum efficiency of 6.4% (V_{oc} of 0.475 V, J_{sc} of 20.4 mA/cm^2, and FF of 0.655), which is 1.5 times higher than that of the control planar solar cell (a maximum η of 4.2%: V_{oc} of 0.470 V, J_{sc} of 13.1 mA/cm^2, and FF of 0.677). Importantly, both solar cells exhibit consistent photovoltaic performance summarized over 20 samples (Supporting Information, Table

S1), which shows the uniform, scalable, and repeatable fabrication of our approach.

The superior photovoltaic properties of the micropillar solar cells are closely related to the better material quality associated with the reduced grain boundary densities within the micropillars (Figure 2). The micropillar solar cells have higher internal quantum efficiency (IQE) than that of the control planar solar cells over the entire wavelength regime (Figure 4e). For the shorter wavelength regime (<390 nm), the IQE is affected by the surface passivation and emitter layer quality. For the longer wavelength regime (>700 nm), the IQE can be affected by the light trapping effect. Nevertheless, the higher IQE values in the intermediate wavelength regime (390−700 nm or less) are mainly attributed to better material quality of the micropillar cell due to the larger effective grain sizes resulting from the reduced grain boundary densities within the micropillars, rather than from the charge-carrier collection process because photogenerated charge-carriers for both cells only need to travel a short distance to reach the p−n junction due to the short absorption depths of the short wavelength light. The enhanced material quality in micropillars can be further tested by comparing the photovoltaic properties of micropillar and planar solar cells without defect passivation by hydrogenation, for which the values of V_{oc} reflect the intrinsic quality of the poly-Si. As shown in Figure 4c (Supporting Information, Table S1), the micropillar solar cells have about 57 mV higher V_{oc} than that of planar cells, in contrast to the comparable V_{oc} values after hydrogenation (Figure 4d). The dark current density (J_o) of the micropillar solar cells, calculated by using the projection area, is about 1.7 times smaller than that of planar cells. Both higher V_{oc} and lower J_o are caused by the larger grain size, not by the radial junction structure since radial junction structures typically result in higher J_o and hence smaller V_{oc} than planar cells due to their larger surface and junction areas.[16,22] Notably, microstructured radial junction solar cells exhibit much higher V_{oc} and lower J_o than the control planar cells, albeit their 6−7 times larger surface and junction area. To further verify that the micropillar solar cells have better material quality, we compared the dependence of the photovoltaic characteristics of the micropillar and planar solar cells (without a-SiN:H and hydrogenation) on the horizontal grain sizes of as-deposited p^{++} poly-Si (Supporting Information, Figure S1). The benefits of the micropillar TFSCs are pronounced when the poly-Si thin-film has smaller grain sizes (2.1 ± 0.3 μm), in that they have about 100 mV higher V_{oc} and 4.2 times higher efficiency than the planar cells, which shows the effective material quality enhancement of the micropillar solar cells. Moreover, as we increased the horizontal grain sizes of the as-deposited p^{++} poly-Si from 2.1 ± 0.3 μm to 5.1 ± 0.4 μm by increasing the flow rate of HCl, the photovoltaic properties of micropillar solar cells are improved at a less degree than those of planar cells in terms of η, V_{oc}, FF, and J_{sc}, which supports that the grain size of micropillars is less sensitive to the initial grain size since the shrinking and subsequent epitaxial growth effectively reduce the grain boundary densities within the micropillars. On the other hand, the higher IQE values in the long wavelength regime (800−1100 nm) for the micropillar solar cells cannot be exclusively explained by the better material quality, since the reduction of the defect density in solar cells typically increases IQE values uniformly,[23,24] unlike the hump shape observed here. Hence, we believe that effective charge-carrier collection process in the radial junction structure of the micropillar solar cells also contributes to the higher IQE values in the long wavelength regime.

In summary, this work takes advantages of the columnar grain structure of the as-deposited p^{++} poly-Si by first forming the p^{++} Si micropillars and then epitaxially growing p-type Si on top, which leads to the fabrication of poly-Si TFSCs on foreign substrates with improved material quality. The resulting micropillar poly-Si TFSCs, compared to the control planar solar cells, have three advantages: (1) enlarged grain size effects due to the Si micropillar seeded epitaxial growth and the corresponding grain boundary density reduction within the micropillars, (2) efficient charge-carrier collection from the radial junction structure, and (3) enhanced light absorption due to reduced light reflection and increased light scattering. As a result, the maximum efficiency of micropillar poly-Si TFSCs (~6.4%) is about 1.5 times higher than that of the control planar ones. The present micropillar poly-Si TFSCs, in comparison to the well-designed and optimized state-of-the-art planar poly-Si TFSCs ($\eta \sim 8.0\%$: V_{oc} of 0.534 V, J_{sc} of 20.7 mA/cm^2, and FF of 0.730),[2] need to be optimized in terms of the poly-Si deposition conditions, the hydrogenation process[25] and the top and bottom electrode design (e.g., interdigitated electrodes)[26] for larger V_{oc} and FF, and the geometric optimization of the micropillar arrays[17] and the employment of the back surface reflector (e.g., alumina substrate)[3] for higher J_{sc}. In addition, efforts are needed to lower the cost from the additional p^{++} growing and etching fabrication steps. Nevertheless, we believe that the shrinking and growing approach can lead to improved grain quality not only for TFSCs, but for many applications involving polycrystalline films, such as thin-film transistors.

Methods. *Fabrication of the Micropillar Poly-Si TFSCs.* *First*, the planar 18 μm thick p^{++} poly-Si thin-film was deposited on a SiO_2 (600 nm)/Si (500 μm) wafer in two consecutive processes: nucleation and growth of poly-Si. The p^{++} poly-Si thin film was nucleated at 1050 °C and 40 Torr with 110 sccm HCl, 100 sccm dichrolosilane (DCS), and 20 slm H_2 gases for 3 min, and grown subsequently at 1050 °C and 60 Torr with 90 sccm HCl, 370 sccm DCS, 110 sccm B_2H_6 (1% diluted in H_2), and 20 slm H_2 gases, which produced a growth rate of about 1 μm/min. The resistivity of the as-deposited p^{++} poly-Si thin-film was about 0.003 Ω·cm. *Second*, the p^{++} poly-Si thin film was photolithography patterned and etched to form p^{++} poly-Si micropillar array (3 μm diameter) by the deep reactive ion etch. The micropillar array was further shrunk to smaller diameter micropillars ($0.8 - 0.9$ μm) by the isotropic dry etch (130 sccm of SF_6 only with a 600 W plasma power). *Third*, the p-type poly-Si absorber layer was grown over the p^{++} poly-Si micropillar arrays at 1050 °C and 60 Torr with 90 sccm HCl, 370 sccm DCS, 110 sccm p-type dopant gas (a mixing ratio of 20% of B_2H_6 (1% diluted in H_2) and 80% of H_2), and 20 slm H_2 gases for 5 min after thermal annealing at 1050 °C and 60 Torr in H_2 environment for 10 min. The resistivity of the as-deposited p-type poly-Si absorber layer was about 0.1 Ω·cm. *Fourth*, the p-n junction was formed using n-type dopant diffusion at 950 °C in N_2 and O_2 environment for 1 min 25 s by flowing N_2 gas through a bubbler filled with $POCl_3$. The resistivity of the n-type poly-Si emitter was about 0.001 Ω·cm. *Finally*, control planar poly-Si thin-film solar cells were fabricated with identical processes without the dry etching step that formed the Si micropillars. Although we grew the p-type poly-Si absorber of the planar and the micropillar array solar cells under identical growth condition and time, the

thickness of the p-type poly-Si of the micropillar solar cells (2.5 μm thickness at the sidewall and 4−5 μm thickness at the top of micropillars) was not identical to that of the planar solar cells (5 μm thickness), due to the limited spacing between micropillars.

The mesa structure of our solar cells was patterned using photolithography, followed by the deep reactive ion etch to expose p^{++} poly-Si layer. The hydrogenation was carried out using the remote H_2 plasma at 450 °C and 230 mTorr using 100 sccm H_2 and 30 sccm Ar with a 300W plasma power (13.56 MHz plasma frequency) for 45 min. After the hydrogenation, the 80 nm thick a-SiN:H layer was deposited at 350 °C and 650 mTorr using 2000 sccm 2% SiH_4 balanced in N_2 and 33 sccm NH_3 with mixed plasma frequencies of 13.56 MHz and 187.5 kHz (the power of both plasma was 20 W and the cycle duration was 5 and 2 s, respectively; deposition rate was about 9.5 nm/min). The refractive index of the deposited a-SiN:H layer was 1.95. The top and bottom contacts were metallized with Ti/Pd/Ag (5/300/700 nm) and Al (700 nm), respectively, using electron beam evaporator after photolithography patterning, followed by the removal of the a-SiN:H and native oxides (soaking in 2% HF). The photoresists were removed by soaking the samples in acetone after the top and bottom contact metallization.

Optical Measurements. The wavelength-dependent light reflection properties were obtained with an integrating sphere using a xenon lamp coupled to a monochromator (model QEX7, PV Measurements, Inc.). In the integrating sphere, a photodetector collected the reflected light from the sample. For the light transmission measurement, the 500 μm thick Si layer underneath the SiO_2 on the original SiO_2/Si growth wafer was removed by KOH wet etch, and the light transmission properties were obtained by comparing the transmission of the samples with a calibrated Si reference photodiode. The light absorption was calculated with the formula, absorption (%) = 100 − reflection (%) − transmission (%). The external quantum efficiencies were first obtained with a xenon lamp coupled to the monochromator (model QEX7, PV Measurements, Inc.), after photocurrents were calibrated with Si photodiodes. The internal quantum efficiencies were then calculated by dividing the external quantum efficiencies by the light absorption percentages.

Solar Cell Characterization. The photovoltaic properties of the solar cells were characterized under AM 1.5G illumination (Class AAA solar simulator, model 94063A, Oriel) after the solar intensity was calibrated with a reference solar cell and a readout meter for solar simulator irradiance (model 91150 V, Newport). The dark and light $J-V$ curves were measured by contacting the top and bottom metal electrodes of the devices with tungsten probes which were connected to a semiconductor analyzer (model 4200-SCS, Keithley). The solar cell area was 1 cm^2, and the J_{sc} and η were calculated on the basis of the active projected area of the solar cells for both the planar and the micropillar solar cells.

■ ASSOCIATED CONTENT

Supporting Information

Dependence of the photovoltaic properties on the horizontal grain sizes of as-deposited poly-Si thin-film for both the micropillar and the planar poly-Si TFSCs, and the averaged photovoltaic properties of the micropillar and the planar poly-Si TFSCs without and with hydrogenation process. This material is available free of charge via the Internet at http://pubs.acs.org.

■ AUTHOR INFORMATION

Corresponding Author

*E-mail: xlzheng@stanford.edu.

Notes

The authors declare no competing financial interest.

■ ACKNOWLEDGMENTS

This material is based upon work supported by the Center on Nanostructuring for Efficient Energy Conversion, an Energy Frontier Research Center funded by the U.S. Department of Energy, Office of Science, Office of Basic Energy Sciences under Award Number DE-SC0001060. D.R.K. and X.L.Z. designed the experiments. D.R.K., C.H.L., J.M.W., I.S.C., and X.L.Z. performed experiments and analyzed the data. D.R.K. and X.L.Z. prepared the manuscript, and all authors discussed the results and commented on the manuscript.

■ REFERENCES

(1) Chopra, K. L.; Paulson, P. D.; Dutta, V. Thin-film solar cells: an overview. *Prog. Photovoltaics: Res. Appl.* **2004**, *12*, 69−92.

(2) Gordon, I.; Carnel, L.; Van Gestel, D.; Beaucarne, G.; Poortmans, J. 8% efficient thin-film polycrystalline-silicon solar cells based on aluminum-induced crystallization and thermal CVD. *Prog. Photovoltaics: Res. Appl.* **2007**, *15*, 575−586.

(3) Beaucarne, G.; Bourdais, S.; Slaoui, A.; Poortmans, J. Thin-film polycrystalline Si solar cells on foreign substrates: film formation at intermediate temperatures. *Appl. Phys. A: Mater. Sci. Process.* **2004**, *79*, 469−480.

(4) Beaucarne, G.; Bourdais, S.; Slaoui, A.; Poortmans, J. Thin-film polysilicon solar cells on foreign substrates using direct thermal CVD: material and solar cell design. *Thin Solid Films* **2002**, *403−404*, 229−237.

(5) Gordon, I.; et al. Three novel ways of making thin-film crystalline-silicon layers on glass for solar cell applications. *Sol. Energy Mater. Sol. Cells* **2011**, *95*, S2−S7.

(6) Green, M. A.; et al. Crystalline silicon on glass (CSG) thin-film solar cell modules. *Sol. Energy* **2004**, *77*, 857−863.

(7) Green, M. A. Thin-film solar cells: review of materials, technologies and commercial status. *J. Mater. Sci.: Mater. Electron.* **2007**, *18*, S15−S19.

(8) Basore, P. A. *Proc. 29th IEEE Photovoltaic Specialists Conf.* **2002**, 49−52.

(9) Brazil, I.; Green, M. A. Investigating polysilicon thin film structural changes during rapid thermal annealing of a thin film crystalline silicon on glass solar cell. *J. Mater. Sci.: Mater. Electron.* **2010**, *21*, 994−999.

(10) Matsuyama, T.; et al. High-quality polycrystalline silicon thin film prepared by a solid phase crystallization method. *J. Non-Cryst. Solids* **1996**, *198−200*, 940−944.

(11) Farrenbruch, A. L.; Bube, R. H. *Fundamentals of Solar Cells: Photovoltaic Solar Energy Conversion*; Academic Press: New York, 1983.

(12) Green, M. A. *Solar cells*; Prentice-Hall: Upper Saddle River, NJ, 1982.

(13) Kayes, B. M.; Atwater, H. A.; Lewis, N. S. Comparison of the device physics principles of planar and radial p-n junction nanorod solar cells. *J. Appl. Phys.* **2005**, *97*, 114302.

(14) Kim, D. R.; Lee, C. H.; Rao, P. M.; Cho, I. S.; Zheng, X. L. Hybrid Si microwire and planar solar cells: passivation and characterization. *Nano Lett.* **2011**, *11*, 2704−2708.

(15) Kelzenberg, M. D.; et al. Enhanced absorption and carrier collection in Si wire arrays for photovoltaic applications. *Nat. Mater.* **2010**, *9*, 239−244.

(16) Garnett, E.; Yang, P. Light Trapping in Silicon Nanowire Solar Cells. *Nano Lett.* **2010**, *10*, 1082−1087.

(17) Alaeian, H.; Atre, A. C.; Dionne, J. A. Optimized light absorption in Si wire array solar cells. *J. Opt.* **2012**, *14*, 024006.

(18) Zhu, J.; et al. Optical absorption enhancement in amorphous silicon nanowire and nanocone arrays. *Nano Lett* **2009**, *9*, 279−282.
(19) Aberle, A. G. Surface passivation of crystalline silicon solar cells: a review. *Prog. Photovoltaics: Res. Appl.* **2000**, *8*, 473−487.
(20) Keevers, M. J.; Turner, A.; Schubert, U.; Basore, P. A.; Green, M. A. *Proc. 20th Eur. Photovoltaic Solar Energy Conf.* **2005**, 1305−1308.
(21) Lindekugel, S.; Lautenschlager, H.; Ruof, T.; Reber, S. *Proc. 23rd Eur. Photovoltaic Solar Energy Conf.* **2008**, 2232−2235.
(22) Boettcher, S. W.; et al. Energy-conversion properties of vapor-liquid-solid-grown silicon wire-array photocathodes. *Science* **2010**, *327*, 185−187.
(23) Terry, M. L.; Inns, D.; Aberle, A. G. Rapid thermal annealing and hydrogen passivation of polycrystalline silicon thin-film solar cells on low-temperature glass. *Adv. OptoElectronics*, Article ID 83657 (**2007**).
(24) Brendel, R.; et al. *Proc. the 26th IEEE Photovoltaic Specialists Conf.* **1997**, 635−638.
(25) Gorka, B.; et al. *Proc. 22nd Eur. Photovoltaic Solar Energy Conf.* **2007**, 2024−2027.
(26) Gordon, I.; et al. Development of interdigitated solar cell and module processes for polycrystalline-silicon thin films. *Thin Solid Films* **2006**, *511−512*, 608−612.